


The conceptual design of 1-ps time resolution neutron detector for fusion reaction history measurement at OMEGA and the National Ignition Facility

Cite as: Rev. Sci. Instrum. **91**, 053306 (2020); <https://doi.org/10.1063/1.5143657>

Submitted: 26 December 2019 . Accepted: 05 May 2020 . Published Online: 27 May 2020

Yasunobu Arikawa , Masato Ota, Makoto Nakajima, Tomoki Shimizu, Sadashi Segawa, Thanh Nhat Khoa Phan, Youichi Sakawa , Yuki Abe , Alessio Morace, Seyed Reza Mirfayzi , Akifumi Yogo, Shinsuke Fujioka , Mitsuo Nakai , Hiroyuki Shiraga, Hiroshi Azechi, Ryosuke Kodama, Koichi Kan , Johan Frenje , Maria Gatu Johnson , Arijit Bose , Neel V. Kabadi, Graeme D. Sutcliffe, Patrick Adrian , Chikang Li, Fredrick H. Séguin, and Richard Petrasso 



View Online



Expert Citation



CrossMark

Lock-in Amplifiers
up to 600 MHz



The conceptual design of 1-ps time resolution neutron detector for fusion reaction history measurement at OMEGA and the National Ignition Facility

Cite as: Rev. Sci. Instrum. 91, 053306 (2020); doi: 10.1063/1.5143657

Submitted: 26 December 2019 • Accepted: 5 May 2020 •

Published Online: 27 May 2020



View Online



Export Citation



CrossMark

Yasunobu Arikawa,^{1,a)} Masato Ota,¹ Makoto Nakajima,¹ Tomoki Shimizu,¹ Sadashi Segawa,¹ Thanh Nhat Khoa Phan,¹ Youichi Sakawa,¹ Yuki Abe,¹ Alessio Morace,¹ Seyed Reza Mirfayzi,¹ Akifumi Yogo,¹ Shinsuke Fujioka,¹ Mitsuo Nakai,¹ Hiroyuki Shiraga,¹ Hiroshi Azechi,¹ Ryosuke Kodama,¹ Koichi Kan,² Johan Frenje,³ Maria Gatu Johnson,³ Arijit Bose,³ Neel V. Kabadi,³ Graeme D. Sutcliffe,³ Patrick Adrian,³ Chikang Li,³ Fredrick H. Séguin,³ and Richard Petrasso³

AFFILIATIONS

¹Institute of Laser Engineering, Osaka University, 2-6 Yamadaoka, Suita, Osaka 565-0871, Japan

²The Institute of Scientific and Industrial Research, Osaka University, 8-1 Mihogaoka, Ibaraki, Osaka 567-0047, Japan

³Plasma Science and Fusion Center at Massachusetts Institute of Technology, 77 Massachusetts Avenue, NW16, Cambridge, Massachusetts 02139-4307, USA

^{a)} Author to whom correspondence should be addressed: arikawa-y@ile.osaka-u.ac.jp

ABSTRACT

The nuclear burn history provides critical information about the dynamics of the hot-spot formation and high-density fuel-shell assembly of an Inertial Confinement Fusion (ICF) implosion, as well as information on the impact of alpha heating, and a multitude of implosion failure mechanisms. Having this information is critical for assessing the energy-confinement time τ_E and performance of an implosion. As the confinement time of an ICF implosion is a few tens of picoseconds, less than 10-ps time resolution is required for an accurate measurement of the nuclear burn history. In this study, we propose a novel 1-ps time-resolution detection scheme based on the Pockels effect. In particular, a conceptual design for the experiment on the National Ignition Facility and OMEGA are elaborated upon herein. A small organic Pockels crystal “DAST” is designed to be positioned ~ 5 mm from the ICF implosion, which is scanned by a chirped pulse generated by a femto-second laser transmitted through a polarization-maintained optical fiber. The originally linearly polarized laser is changed to an elliptically polarized laser by the Pockels crystal when exposed to neutrons, and the modulation of the polarization will be analyzed. Our study using 35-MeV electrons showed that the system impulse response is 0.6 ps. The response time is orders of magnitude shorter than current systems. Through measurements of the nuclear burn history with unprecedented time resolution, this system will help for a better understanding of the dynamics of the hot-spot formation, high-density fuel-shell assembly, and the physics of thermonuclear burn wave propagation.

Published under license by AIP Publishing. <https://doi.org/10.1063/1.5143657>

I. INTRODUCTION

The generation of nuclear fusion energy has been one of humanity’s biggest challenges. In the coming years, magnetic confinement fusion and inertial confinement fusion (ICF) generate plasmas that approach the required conditions for fusion ignition and energy gain. The most viable fuel for energy applications is

deuterium–tritium (DT) fuel, and in DT fusion reactions, alpha particles and neutrons are produced via $D + T \rightarrow He + n + 17.6$ MeV, where alpha particles heat up the fuel and boost the yield. If the alpha heating exceeds the cooling of the plasma fuel, a self-sustaining fusion reaction will be realized, which is called “ignition.” Recent National Ignition Facility (NIF) experiments have achieved significant alpha heating where the fusion neutron yields increased

with a factor of 2.9 compared to the non-alpha heating conditions.^{1,2} A prerequisite for achieving ignition conditions is to obtain a fundamental understanding of the dynamics of the hot-spot formation and high-density fuel-shell assembly as well as the temporal evolution of the alpha heating in an ICF implosion.

In NIF fusion experiments, laser pulses with 15 ns pulse-duration are typically used to irradiate a capsule filled with DT fuel.³ When the fuel is compressed, the ion temperature (T_i) and density (ρ) of the fuel increase and initiate fusion reactions, leading to generation of neutrons, as discussed above. The peak time of the neutron production is called “bang time.”⁴ After maximum compression of the fuel, which can occur before or after bang time, depending on the performance of the implosion, the plasma starts expanding, resulting in reduced T_i and ρ that quench the fusion process. Figure 1 shows the results from 2D hydrodynamic simulations reported by Frenje *et al.*,⁵ which illustrate the nuclear burn history, T_i , and areal density (ρR) of a typical NIF implosion. Figure 1(a) shows the case without alpha heating, 1(b) shows the same implosion when alpha heating was artificially enhanced four times, and 1(c) shows the implosion when alpha heating was artificially enhanced 88 times, necessary for ignition to occur. In Fig. 1(d), the nuclear burn history (or rather the neutron emission history) kept increasing after the peak compression; however, the alpha heating was not enough to overcome the energy losses. In Fig. 1(c), the alpha heating exceeds the cooling losses, and the neutron emission history kept increasing, sustained by the T_i increase after peak compression. The durations of the emission histories are on the order of 100 ps for the failed implosions and ~ 40 ps for the ignited implosion, and the reaction rate is increased by two orders of magnitude when alpha heating overcomes the energy losses. Recent studies are trying to understand the unknown mechanisms responsible for the ignition failures, such as unknown energy losses due to the mixing of high-Z impurity from the hydro instabilities^{8,9} and possibly multi-ion separation issues.^{6,7} High-mode turbulence with a time scale of less than 10 ps has been observed in high-resolution 3D hydrodynamic simulations,¹⁰ which indicates that a few ps diagnostic time resolution is required. Recent advances in the numerical simulations have enabled this type of physics to be implemented into codes to reproduce some of the observations. Unfortunately, most current experimental studies rely on time-integrated observations, such as total neutron yield or neutron burn-averaged T_i , making it difficult to validate the numerical modeling of the implosion dynamics. As shown by Fig. 1, for instance, the neutron emission history is changing significantly with an increasing in alpha heating. To probe the dynamics of an implosion in detail, we need to measure the neutron emission and T_i histories with a time resolution of a few ps.

Nuclear burn history has been diagnosed for decades.^{11–16} So far, the fastest neutron detector response time was 27 ps and 25 ps achieved by Azechi *et al.* in 1989¹¹ and Lerche *et al.* in 1995¹² for non-cryogenic DT implosions, respectively, and 70-ps for a cryogenic DT implosion,¹⁵ which depends on the distance between the implosion and the detector. Recently, a 10-ps time resolution γ -ray burn history detector, known as the pulse dilation gas Cherenkov detector,¹⁶ was developed on the NIF.

In this paper, we describe a conceptual design of a detector for the measurements of the nuclear burn history in a cryogenic DT

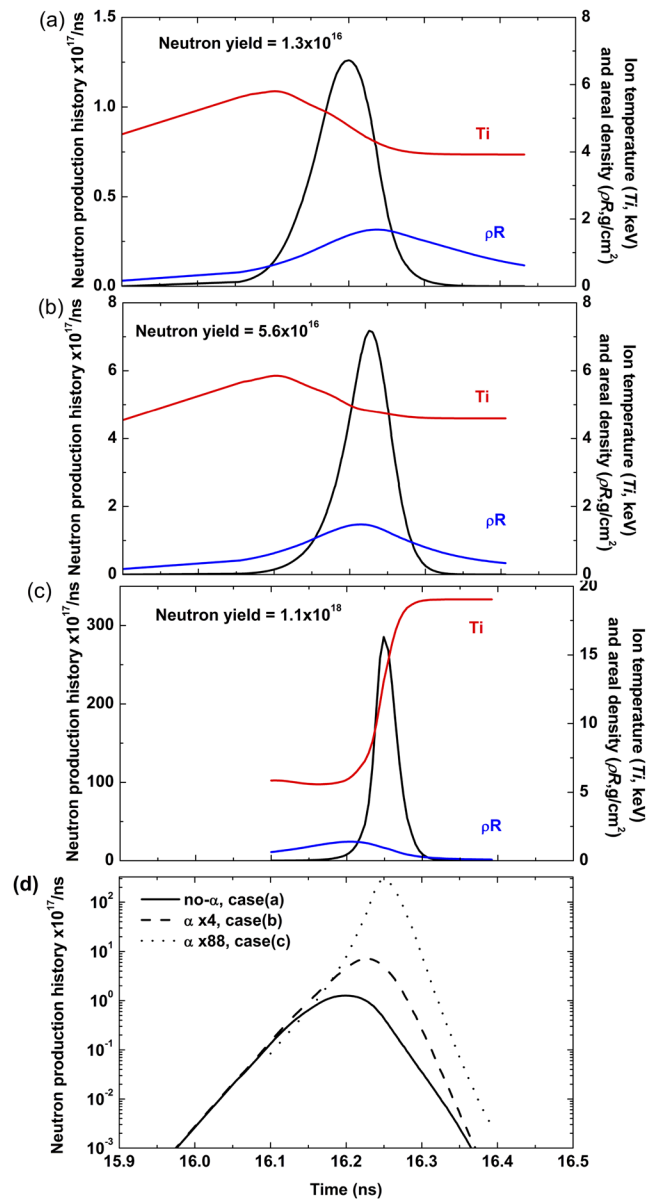


FIG. 1. Simulated nuclear burn history and evolution of T_i and ρR for three types of implosions: (a) with no alpha heating, (b) with a small amount of alpha heating, and (c) with significant alpha heating for it to ignite. (d) The nuclear burn histories for the three cases. $t = 0$ ns represents the beginning of the laser irradiation.

implosion with 1.4 ps time resolution at OMEGA and the NIF. In Sec. II, the requirements for the burn history measurement and limiting factors are described. Section III discusses the principle of the Pockels effect scanning technique. In Sec. IV, the conceptual design of the system is elaborated upon. Sections V and VI describe the impulse response and signal intensity. In Sec. VII, the background level is discussed, and Sec. VIII summarizes this work.

II. DIAGNOSTICS REQUIREMENT FOR BURN HISTORY MEASUREMENTS

Current detectors typically have a few tens of picosecond response time, and these detectors have been used to measure part of the actual nuclear burn history. With these detectors, the burn width (FWHM) is measured with an accuracy of 10–20-ps. The assessment of finer structures of the burn history requires much faster response times on the order of a few ps.

Conventional high-speed neutron detectors have relied on plastic scintillators, light transmitting optics, and a streak camera. The BC-422 scintillator is known as the fastest-response plastic scintillator with a rise time of 10–30 ps and a fall time of 2.5 ns.^{11,12,14} There are a few reports of faster time scintillator materials (few ps),¹⁷ but these scintillators do not generate sufficient amount of light and are not useful for the application discussed herein.

The measured nuclear burn history is temporally broadened by the detector response and neutron energy spectrum (with a certain spectral width). The FWHM of the neutron spectrum is mainly dictated by the Doppler broadening, which can be translated to a temporal broadening at the detectors, as described by^{12,18}

$$\Delta t = 0.122 \cdot \sqrt{T_i} \cdot d \text{ for } D + T \rightarrow {}^4\text{He}(3.5 \text{ MeV}) + n(14.1 \text{ MeV}), \quad (1)$$

$$\Delta t = 0.778 \cdot \sqrt{T_i} \cdot d \text{ for } D + D \rightarrow {}^3\text{He}(0.8 \text{ MeV}) + n(2.5 \text{ MeV}), \quad (2)$$

where the coefficients 0.122 and 0.778 are given in $\text{keV}^{-1/2} \text{ s m}^{-1}$, Δt is the FWHM of the temporal broadening given in ps, T_i is given in keV, and d is the distance between the implosions and the detector (given in mm). Typical NIF-implosion conditions, shown in Fig. 1(b), show a T_i of about 5 keV at bang time. Under these conditions, the neutron detector must be placed at 5 mm from the implosion to measure the burn history with a time resolution of 1 ps.

III. ULTRAFAST DETECTION USING POCKELS EFFECT

The Pockels effect is known as an electro-optic (EO) effect with a very fast response time of about 10 fs, which is generally limited by the duration of the laser pulse. The method of femtosecond EO sampling is widely used for detection of the electric field generated by terahertz waves and electron-bunch.^{19–24} For the measurement of the electron bunches, less than 100 fs time resolution have been reported from free electron accelerator experiments^{25,26} or experiments with ultra-intense-laser generated electron beams.²⁷ When an electric field is generated in the Pockels crystal, the polarization of the laser traveling through the crystal is rotated by the Pockels effect. The generated electric field in the crystal can be measured from the modulation amplitude of the polarization component with a time resolution of ~ 10 fs. Furthermore, using an optical chirped pulse laser, the time history of the EO signals can be translated to the wavelength spectrum that can be measured very accurately with spectrometers²⁵ (see Fig. 2). In this paper, we propose a new system that can measure the electric field induced by neutrons with a time resolution of ~ 1 ps.

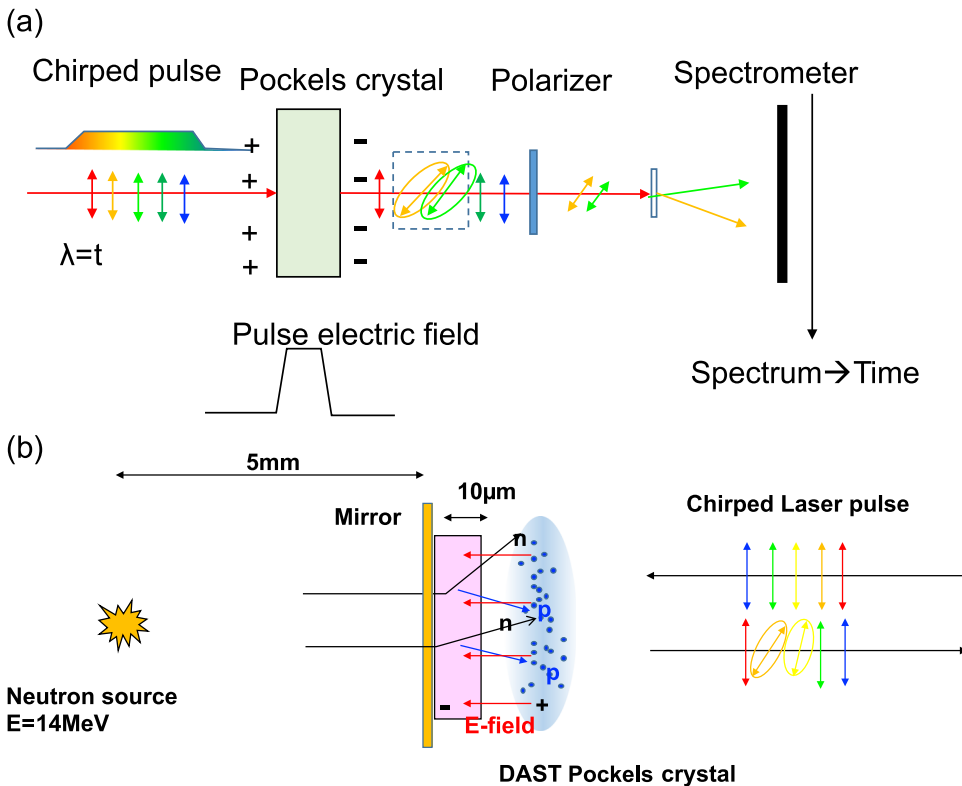


FIG. 2. (a) Schematic drawing illustrating the principle of the single-shot electric-field detection via the Pockels effect and (b) drawing of using this scheme for neutron detection.

The DAST [*trans*-4'-(dimethylamino)-*N*-methyl-4-stilbazolium tosylate, $C_{23}H_{26}N_2SO_3$] crystal is²⁸ an organic crystal, which has the largest EO coefficient. Since DAST contains abundant of hydrogen in the material, it has an intrinsic sensitivity for neutrons. Conversely, its low Z number makes it less sensitive to x rays. When neutrons interact with the thin DAST crystal, recoil protons are generated and ejected while electrons stay put. The charge separation creates an electric field in the DAST crystal along the opposite direction of the incoming neutrons, as shown at Fig. 2(b). This electric field includes the temporal information of the produced neutrons and can be measured with the EO sampling technique. Instead, choosing a Pockels crystal with a high Z number will effectively allow measurements of γ -rays, since γ -rays generate electrons, which, in turn, generate an electric field. Since γ -rays relax the temporal broadening constraint, this is another interesting route to measure the burn history.

IV. EXPERIMENTAL MEASUREMENT OF THE EO SAMPLING IMPULSE RESPONSE

Since access to experiments at the NIF or OMEGA is quite limited, experiments evaluating the EO-sampling response time was evaluated by using a short pulse electron beam. A 1-ps pulse duration electron beam was produced with a linear accelerator (LINAC) at Osaka University. A Ti:sapphire femtosecond laser system was also used for these experimental tests.

The physical principle of EO-detection using electrons is slightly different from that of neutrons; in the neutron-detection case, recoil protons generate an electric field and EO modulations, while in the electron-detection case, an electric field and EO modulations are created by electrons passing beside the crystal. To fully test the technique with neutrons, an intense neutron source is essentially needed, but it is extremely hard to access such an intense neutron source. Since the electron pulse is very well controlled in terms of pulse duration, it is worth doing an actual experiment using electron beams. In this experiment, an electron beam of 2.5×10^9 electrons with a pulse-duration of about 1 ps, and an energy of 35 MeV, was injected 2.4 mm above the zinc telluride (ZnTe) (110) Pockels crystal. This crystal had a size of $10 \times 11 \times 1$ mm,³ as shown in Fig. 3(a). A vertically line polarized laser with 100-fs pulse duration was injected. The laser injection time was scanned against the electron injection time with a time step of 0.2 ps by using an optical delay stage. The laser pulse was divided into two perpendicular polarization components by using a polarization beam splitter, and they were measured with photo diode detectors. A $1/4 \lambda$ phase plate was installed to change the initially line polarized beam to a circular polarized beam, and the phase shift induced by the Pockels effect was measured by using two photo detectors. The signal intensity vs delay time is shown in Fig. 3(b). The ZnTe (110) surface crystal was chosen because it is one of the most well-known EO sampling crystals to detect an electric

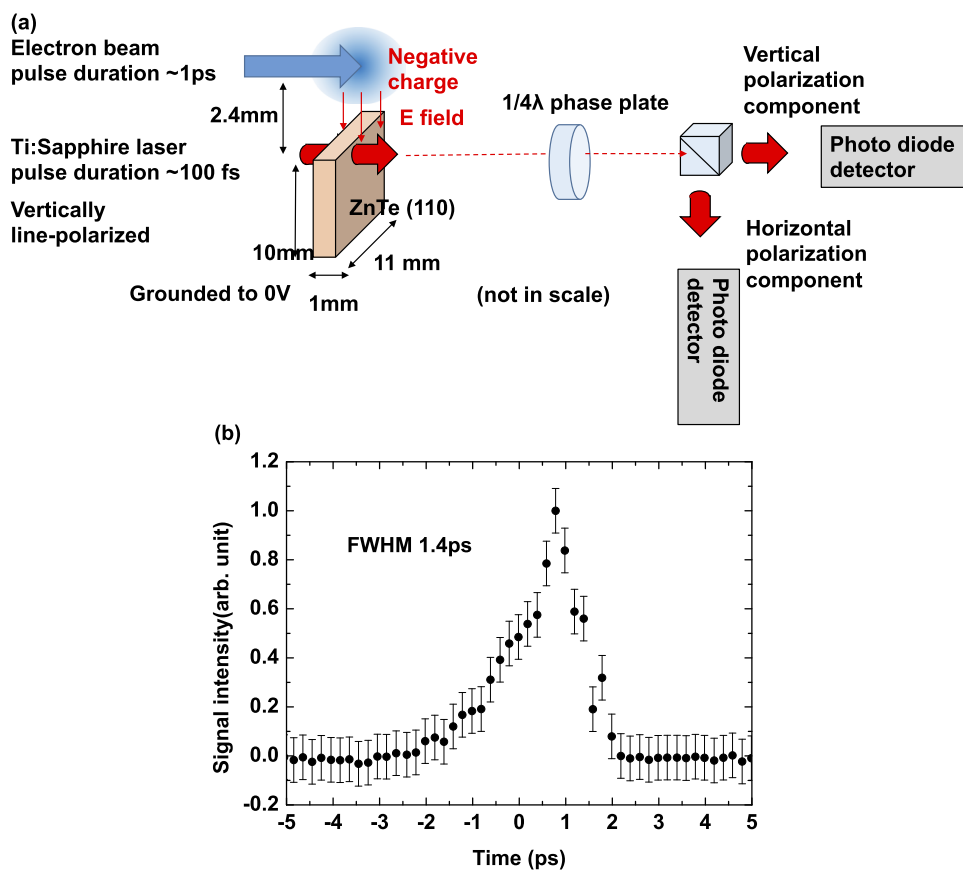


FIG. 3. (a) Experimental setup and (b) the EO sampling impulse response.

field. A 1.4-ps FWHM impulse response was observed. Considering the uncertainty in the measurement, the polarization-rotation angle obtained in the experiment was reproduced by the model calculation described by formulas (12)–(14); the experimentally observed polarization-rotation angle was 0.54 ± 0.04 rad, while the model calculated was 0.28–0.64 rad. The error of the experiment is dictated by the signal wave fluctuation and uncertainties in the shape of the electron charge distribution. The model calculation predicts a voltage in the ZnTe crystal of 1200–2800 V, dependent on the dimensions of the ZnTe crystal. The factors used in the formulas were 4.0 pm/V EO coefficient for ZnTe and a refractive index of 2.85. The agreement between the experiment and the model calculation confirms the feasibility of this type of neutron detector for the NIF and OMEGA.

V. CONCEPTUAL DESIGN FOR NIF

The conceptual design of the detector is shown in Fig. 4, which illustrates the scenario where the neutron-induced proton cloud creates an electric field via charge separation in the DAST crystal. The chirped pulse laser passes through the crystal and returns by reflection of the mirror. Figure 4 shows the envisioned detector schematic. The plan is to position the Ti:sapphire laser, based on a chirped pulse with a pulse duration of ~ 300 ps, in an electromagnetic shielded room. The laser pulse will be transmitted through a polarization maintaining fiber (PM fiber) to the crystal.

Typically, a Ti:sapphire laser has a wavelength bandwidth of 100 nm with a center wavelength of 800 nm.

The small DAST crystal assembly is attached to the PM-fiber and positioned 5 mm from a NIF implosion outside the *Hohlraum* wall. In experiments at OMEGA, a similar assembly is attached to the stalk where the crystal will be positioned 2 mm from the implosion. As shown in Fig. 4, the diameter of the assembly is about 0.1 mm. The thickness of the DAST is $10 \mu\text{m}$, not to affect the time resolution. The crystal orientation and cutting angle of the DAST are complex, and there are no experimental demonstrations in this geometry in Fig. 4; thus, it will be optimized in our future work. The reflected laser pulse, which will pass through the DAST crystal, will be analyzed with a polarizer and a spectrometer. A set of perpendicular orientation polarizers will eliminate unwanted light with the incorrect polarization. The spectrometer resolves the spectrum with a resolution of 0.1 nm, and this wavelength resolution over a 100-nm bandwidth corresponds to 0.3-ps time-resolution with a 300-ps time window. By positioning two crystals at different distances (for instance, 5 mm and 50 mm) from the implosion, the temporal evolution of Ti can, in principle, be measured.

VI. IMPULSE RESPONSE

The total impulse response of the system was estimated by convolving (1) the neutron temporal broadening caused by plasma

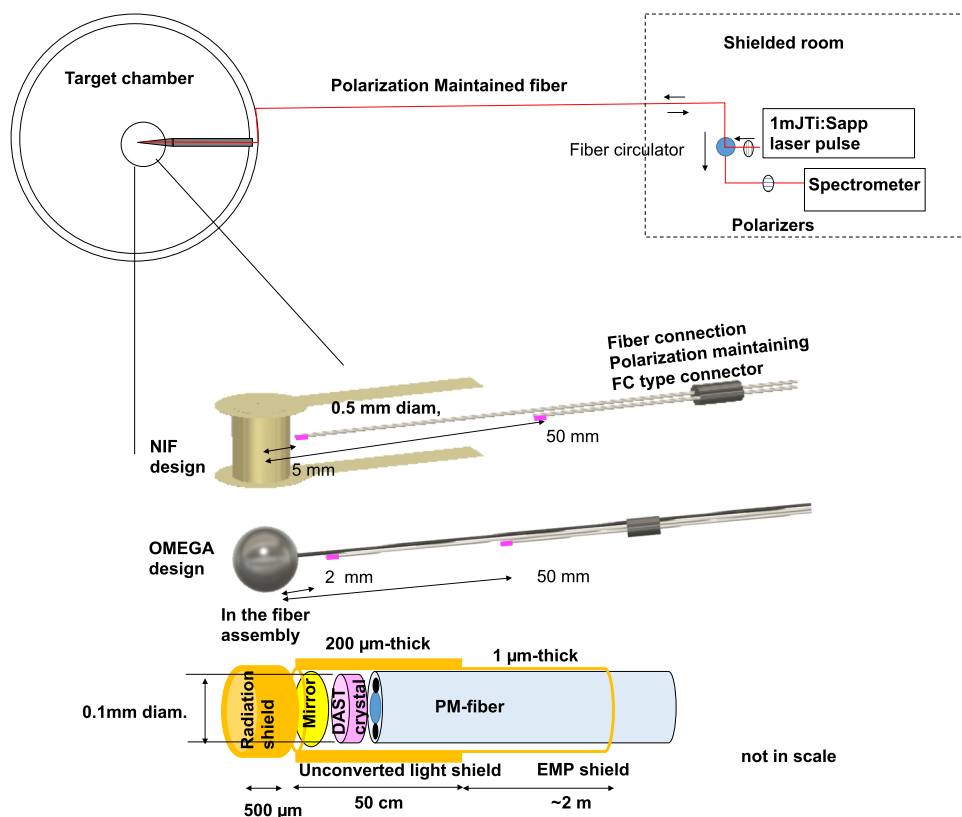


FIG. 4. The conceptual design of the 1-ps time resolution neutron detector at NIF/OMEGA.

Doppler broadening, (2) the time spread in the electric field generation, and (3) the electro-optical-sampling broadening. For a 5-keV plasma, the neutron temporal broadening is 1.3 ps at a detector positioned at 5 mm, while the electro-optical-sampling broadening was established in previous studies to be 0.3 ps. The time spread in the electric field generation was estimated by using the Monte Carlo code PHITS,²⁹ which simulates neutron-induced nuclear reactions, based on the JENDL cross section. In the simulation, a DAST crystal was modeled as 1 g/cm³ CH with a diameter of 1 mm and thickness of 10- μ m, labeled as “DAST.” The other components of

“Vacuum,” “Gap,” and “Fiber” were modeled as vacuum for simplicity. An impulse 14-MeV neutron beam hit the DAST crystal. The images of the generated recoil protons, with a 0.1-ps time step between each image, are shown in Fig. 5(a). The recoil protons generated in the DAST crystal generate a charge separation on a very short time scaled at the back surface of the DAST crystal. Here, we assumed that there is no time delay between the proton and electric-field generation. The electrons remaining in the DAST crystal was assumed to be grounded by the surrounding-metallic component. The simulated time spread in the electric field generation is shown by

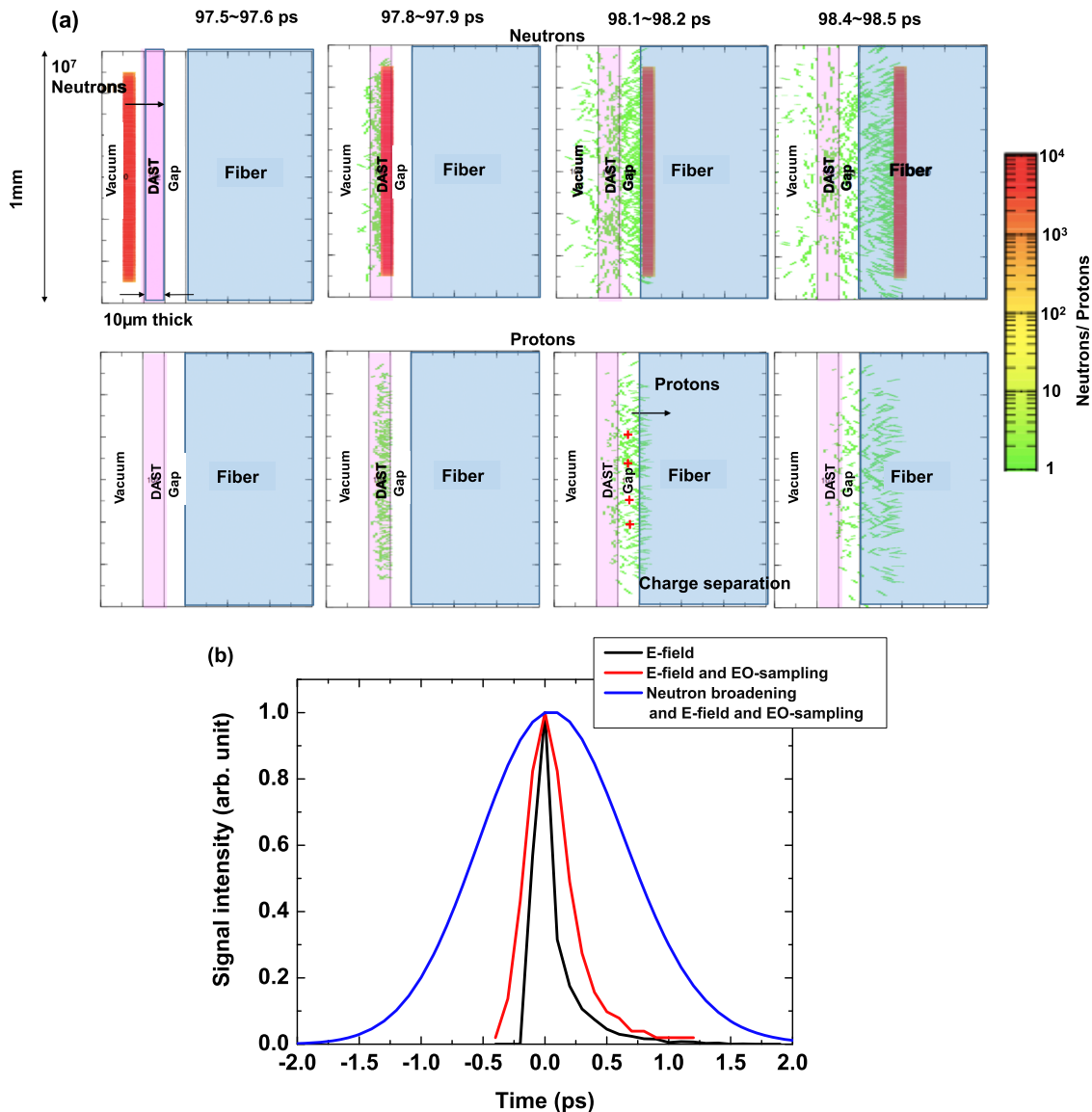


FIG. 5. (a) Monte Carlo simulation of the recoil-proton generation in the DAST crystal, induced by 14-MeV neutrons produced in a 5-keV plasma. (b) The detector impulse response to the neutrons. In this calculation, it was assumed that the DAST crystal was positioned 5 mm away from the implosion. The black curve only considers the time spread in the electric field generation, while the red curve also considers the sampling time spread. The total impulse response is shown by the blue curve, which also considers the Doppler-induced temporal broadening. Table I summarizes the impulse-response data for neutron and gamma-ray measurements.

the black curve in Fig. 5(b). By convolving this signal with the sampling broadening, a system impulse response of 0.6 ps (FWHM) was obtained, as shown by the red curve in Fig. 5(b). Taking into account the neutron temporal broadening at the detector, the total impulse response was estimated to be 1.4 ps, which is an order of magnitude shorter than the current methods. Table I summarizes the impulse-response data for neutron and gamma-ray measurements.

This detector can be also used to detect γ -rays via the $D + T \rightarrow {}^5\text{He} \rightarrow {}^5\text{He} + \gamma$ (16.7 MeV) reaction to provide an alternative nuclear burn history measurement.¹⁶ Since γ -rays do not exhibit any temporal broadening and the fact that they create electrons via indirect ionization of the crystal at a speed of light, only the electro-optical-sampling significantly affects the impulse response for fusion γ -ray measurement, which was estimated to be about 0.3 ps.

The temporal evolution of Ti during burn can also be unfolded as follows: The detected signal can be written as a convolution of pure *Burn History* and *Doppler Broadening* as a function of time,

$$\text{Sig}(t) = \text{Burn History}(t) \otimes \text{Doppler Broadening}(t), \quad (3)$$

where *Doppler Broadening*(t) is a time dependent function, as described by

$$\text{Doppler Broadening}(t) = \exp\left(\frac{-t^2}{2\tau(t)^2}\right), \quad (4)$$

where $\tau(t)$ is the width of Doppler broadening as a function of time [see Eq. (1)],

$$\tau(t) = 0.42 \cdot 0.122\sqrt{\text{Ti}(t)} \cdot d, \quad (5)$$

where 0.42 is from $1\sigma = 0.42$ FWHM of the Gaussian function. With two detectors positioned at different distances, for instance, at 5 mm and 50 mm, the evolution of ion temperature $\text{Ti}(t)$ can be derived as follows:

$$\text{Sig}_{5\text{mm}}(t) = \text{Burn History}(t) \otimes \text{Doppler Broadening}_{5\text{mm}}(t), \quad (6)$$

$$\text{Sig}_{50\text{mm}}(t) = \text{Burn History}(t) \otimes \text{Doppler Broadening}_{50\text{mm}}(t), \quad (7)$$

$$\text{Doppler Broadening}_{5\text{mm}}(t) = \exp\left(\frac{-t^2}{2\tau_{5\text{mm}}(t)^2}\right), \quad (8)$$

$$\text{Doppler Broadening}_{50\text{mm}}(t) = \exp\left(\frac{-t^2}{2\tau_{50\text{mm}}(t)^2}\right), \quad (9)$$

$$\tau_{5\text{mm}}(t) = 0.42 \cdot 0.122\sqrt{\text{Ti}(t)} \cdot 5, \quad (10)$$

$$\tau_{50\text{mm}}(t) = 0.42 \cdot 0.122\sqrt{\text{Ti}(t)} \cdot 50. \quad (11)$$

TABLE I. Neutron and gamma-ray impulse response.

	Impulse response (FWHM) (ps)	Response function for Ti = 5 keV plasma (FWHM) (ps)
Neutron (t)	0.6	1.4
Ti (t)	0.6	1.4
γ (t)	0.3	0.3

VII. SIGNAL INTENSITY ESTIMATION FOR A DETECTOR ON THE NIF AND OMEGA

The signal intensity and temporal distribution generated in a 10- μm thick, 100- μm diameter DAST crystal located at 5 mm from an implosion at the NIF were estimated as follows: By using PHITS simulation, the number of generated recoil protons in the DAST crystal was calculated to be 2×10^8 in total and 3×10^6 protons/1 ps at bang time for a neutron yield of 5.6×10^{16} and a pulse duration of 70 ps [based on Fig. 1(b)].

The voltage (V) generated in the DAST crystal was simply estimated by using a capacitor model, where surface charges +Q and -Q are facing each other with a distance d , the surface area S , and capacitance C , as a function of Q,

$$Q = CV = \frac{k\epsilon_0 S}{d} V; \quad (12)$$

thus,

$$V = \frac{Qd}{k\epsilon_0 S}, \quad (13)$$

where $Q = 3 \times 10^6 \times 1.6 \times 10^{-19}$ C, k is the dielectric constant of the DAST crystal $k = 3$, ϵ_0 is an electric constant of the vacuum $\epsilon_0 = 8.85 \times 10^{-12}$ F/m, $d = 10^{-5}$ m, and $S = \pi \times (5 \times 10^{-5})^2$ m². With these values, we obtain $V = 23$ V at bang time. The electric voltage creates polarization rotation of the laser light, and the polarization angle $\Delta\theta$ after the DAST is given by

$$\Delta\theta = 2\pi n^3 r_{EO} V / \lambda, \quad (14)$$

where a factor of two captures the fact that the laser passes through the DAST crystal twice because of the mirror, n is the refractive index of the DAST crystal, r_{EO} is the electro optical coefficient, V is electric voltage, and λ is the wavelength of the laser. Here, $n = 2.5$, $r_{EO} = 92$ pm/V, and $\lambda = 8 \times 10^{-7}$ m. Then, $\Delta\theta$ at the peak time was estimated to be 0.26 radian. Given that the optical signal intensity after the polarizer can be written as

$$I = I_0 \cdot \sin^2(\Delta\theta), \quad (15)$$

where I_0 is the input laser intensity, an intensity of $I_{sig} = 0.066 \cdot I_0$ is estimated.

The base line intensity is set by the un-modulated laser transmitted through the polarizer and is about 3×10^{-4} (-35 dB). This light is mainly caused by imperfect polarization after the PM-fiber (which is defined as the polarization extinction ratio). In other words, $I_{Baseline} = 3 \times 10^{-4} \cdot I_0$. A typical Ti:sapphire laser with the spectrum correction system can generate pulses with 5% intensity-modulation, as shown in Fig. 6 with a red solid line. The burn history of Fig. 1(b) and the detector response of Fig. 5 (blue curve) were convoluted to calculate the expected signal. Figure 6 shows expected signals for the neutron yield of $Y_n = 5.6 \times 10^{16}$ (black solid curve), 2.8×10^{15} (black dotted curve), and 3.9×10^{17} (black dash curve) and the base line laser in red dash line. The lower detection limit of the neutron yield was estimated to be $\sim 2.8 \times 10^{15}$, having $S/Baseline \sim 1$. The upper limit is $\sim 3 \times 10^{17}$ when $\Delta\theta$ becomes $\sim \pi/2$. For instance, a 1-mJ/300 ps Ti:sapphire laser pulse at the DAST crystal will create 18 μJ signal light (9×10^{13} photons) at the DAST crystal, and then, a sufficient signal can be estimated at the detector with a standard spectrometer. Thus, the dynamic range of the system is more

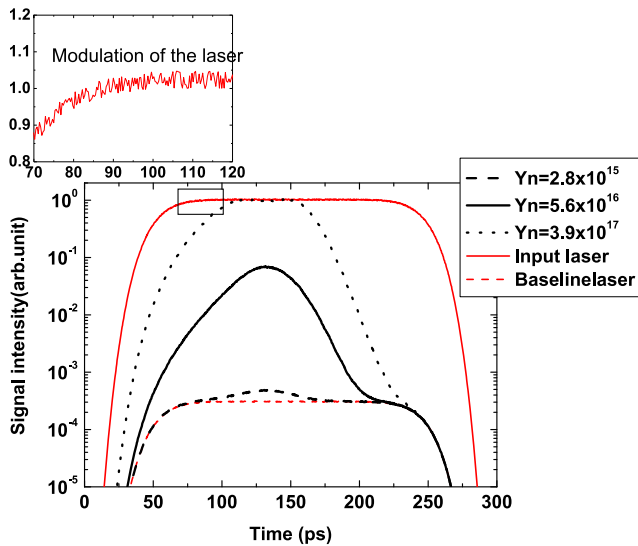


FIG. 6. Temporal distribution of the signal intensity for the neutron yield of $Y_n = 5.6 \times 10^{16}$, 2.8×10^{15} , and 3.9×10^{17} and a 5%-modulation of the laser intensity.

than ~ 100 times, which is adequate for the NIF experiments shown in Fig. 1.

In an OMEGA experiment, the neutron yield is typically in the range of $\sim 10^{13}$ to 1×10^{14} , which dictates the design of the diagnostic. The number of generated recoil protons is proportional to the solid angle efficiency and thickness of the DAST crystal, which means that

$$Q \propto \frac{S}{4\pi R^2} \times d, \quad (16)$$

$$V = Qd/\epsilon_0 S, \quad (17)$$

where Q is charge, R is the distance between the implosion and the DAST crystal, S is the area of the DAST crystal, d is the thickness of the DAST crystal, and V is the voltage applied to the DAST crystal. In other words, V is a function of d and R ,

$$V \propto \frac{d^2}{R^2}. \quad (18)$$

By decreasing R from 5 mm to 2 mm and increasing d from $10 \mu\text{m}$ to $100 \mu\text{m}$, we obtain the same S/B for the OMEGA system as for the NIF system for the neutron yield range of 4.5×10^{12} to 6.2×10^{14} . The detector response time is increased to about 5 ps.

VIII. BACKGROUND ESTIMATION

There are several sources of background that need to be considered in our estimation of the signal-to-background (S/B). The electric field generated by laser-plasma interactions³⁰ will also create a strong EO-signal. To eliminate most of the backgrounds, the DAST crystal will be covered by Au, as shown in Fig. 4, and have shielding for the Electro Magnetic Pulse (EMP), unconverted light shield, and radiation shield.

In the case of the EMP, the shield will be made of Au and be 2-m long and $1 \mu\text{m}$ -thick with $100 \mu\text{m}$ inner diameter. Reference 30

showed that the amplitude of $\sim \text{MV}$ and frequency more than GHz of the EMP can be generated at the laser-interaction point. The diameter of the Au shield entrance hole must be $100 \mu\text{m}$, which will cut the EMP wavelength larger than $100 \mu\text{m}$ or less than 0.3 ps period (3 THz), which is outside the detection range of our system. Furthermore, the 2 m-long Au shield will delay the EMP propagation with 13 ns while traveling to the DAST crystal, which is more than adequate for the burn-history measurement.

The unconverted laser light (with the wavelength of 1053 nm)³¹ will hit the PM-fiber or assembly and affect the measurement. The fiber assembly must be located within the *Hohlraum* supporting arms to avoid direct exposure of the unconverted light. However, still 10% of the unconverted light may hit the fiber assembly. To protect against this light, a 10 cm long, $200 \mu\text{m}$ -thick Au shield will cover the DAST crystal. The shock propagation time from the surface of the Au shield to the DAST crystal was estimated with the 1D hydrodynamic simulation ILESTA³² to be 4 ns relative to the backend of the laser irradiation, which is adequate. In addition, the spectral analyzer should be shielded against 1053 nm stray light by using an 800-nm region bandpass filter.

Soft x rays (in the keV range), hot electrons, or high-energy ions having $\sim \text{MeV}$ can be generated in the implosion experiment,³³ which could generate additional background. The $500\text{-}\mu\text{m}$ thickness Au can shield against most of the particles; the mean free path for electrons and protons are $500\text{-}\mu\text{m}$ in Au 1.5 MeV and 18 MeV, respectively. Thus, most of the electrons and ions are absorbed by the shield. These particles, however, heat up the Au shield, generating shock. Reference 33 indicated that 10% of the laser energy is converted to the radiation, and then, the energy flux of the radiations is around $10 \text{ TW}/\text{cm}^2$ at the Au shield. $500 \mu\text{m}$ thick Au can delay the propagation of the shock for more than 20 ns, which is sufficiently long to protect the DAST crystal. The soft x rays can be attenuated by the 500-thick Au shield; however, hard x rays (with the energy more than MeV) and γ -rays can pass through this shield and interact with the DAST crystal. As they generate electrons in the DAST crystal, an electric field will also be generated by this type of background. There are three sources of x-ray background that must be considered: (1) *Hohlraum* x rays, (2) DT fusion γ -rays with 16.7 MeV, and (3) secondary γ -ray yield from $n(n', \gamma)\text{C}$ and $n(n', \gamma)\text{Au}$ of the *Hohlraum*. Figure 7(a) compares the number of x rays/ γ -rays and DT neutrons as well as down-scattered neutrons.³⁴ The DT of the γ yield was estimated by using the branching ratio for the different reactions,³⁵ i.e., 2.5×10^{-5} lower than the total DT neutron yield. The secondary γ -ray yield from $n(n', \gamma)\text{C}$ and $n(n', \gamma)\text{Au}$ of the *Hohlraum* was estimated to be 2.6×10^{-2} lower than the total DT neutron yield.³⁵ The *Hohlraum* x rays are also generating background, and this component was estimated from the information in Ref. 36. The temporal distributions of these background components are shown in Fig. 7(a), while in Fig. 7(b), the temporal distribution of the signal is compared to the background of the temporal distribution. As illustrated by Fig. 7(b), the signal is more than an order of magnitude larger than the background. Given that the DAST is positioned close to the *Hohlraum*, background radiation from the NIF target chamber or surrounding construction will arrive much later than DT neutrons and thus will not be a problem.

These counter measures for the backgrounds are essential and must be experimentally tested.

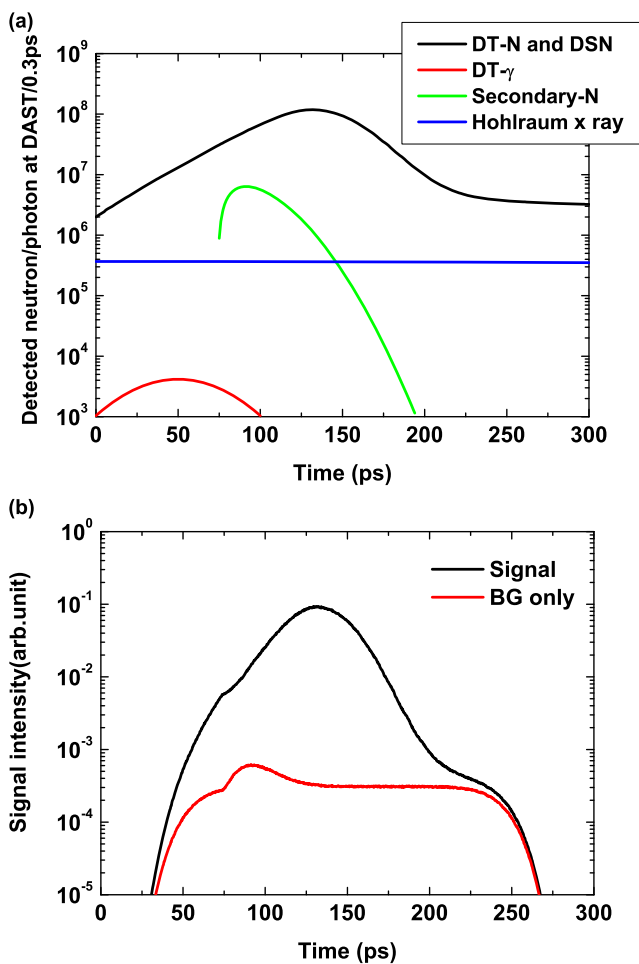


FIG. 7. (a) The temporal distributions of the different backgrounds for the NIF with the neutron yield of 5.6×10^{16} with typical backgrounds, where 50 ps is the γ -ray arrival time at the DAST crystal. (b) Expected temporal distributions of the signal (black) and background (red).

IX. SUMMARY

A new neutron detector for the measurement of nuclear burn histories at the NIF and OMEGA is proposed. This system will provide a time resolution of 1.4 ps, including the neutron temporal broadening, an order of magnitude faster than the current detectors. A small organic “DAST” Pockels crystal is attached to a polarization-maintaining optical fiber, and two crystals will be positioned 5 mm and 50 mm away from the target. Fusion neutrons create recoil protons in the DAST crystals, generating an electric field with a very short time period. A 1 mJ Ti:sapphire laser stretched to ~ 300 ps will be used to probe the electric field generated in the crystal. This study shows that a 0.6-ps impulse response and 1.4-ps time resolution (when considering the neutron temporal broadening at the detector) can be achieved at typical NIF and OMEGA experimental conditions with a good signal to background ratio. From the two detectors positioned at different distances, the evolution of the

ion temperature can be measured with this type of time resolution. Backgrounds were estimated to be sufficiently small. This system has the potential to revolutionize the nuclear burn history measurements at the NIF and OMEGA, enabling unprecedented studies of the fusion burn wave propagation. With an improved sensitivity, improving the scheme can be also utilized at GEKKO-XII or any ICF facilities, or short pulse neutron facilities. Furthermore, a similar technique can be applied for charged particle diagnostics such as electron spectrometers, proton spectrometers, or Thomson parabolas.

ACKNOWLEDGMENTS

This work was funded by the Grant-in-Aid for Scientific Research of MEXT 19H01876, JST A-STEP, the Research Program of the National Institute for Fusion Science (Grant Nos. 2019NIFS16KUGK100 and 2019NIFS18KUGK125), and the Japan-U.S. Cooperation in Fusion Research and Development FP6-4.

REFERENCES

- ¹O. A. Hurricane, D. A. Callahan, D. T. Casey, E. L. Dewald, T. R. Dittrich, T. Döppner, S. Haan, D. E. Hinkel, L. F. Berzak Hopkins, O. Jones, A. L. Kritcher, S. Le Pape, T. Ma, A. G. MacPhee, J. L. Milovich, J. Moody, A. Pak, H.-S. Park, P. K. Patel, J. E. Ralph, H. F. Robey, J. S. Ross, J. D. Salmonson, B. K. Spears, P. T. Springer, R. Tommasini, F. Albert, L. R. Benedetti, R. Bionta, E. Bond, D. K. Bradley, J. Caggiano, P. M. Celliers, C. Cerjan, J. A. Church, R. Dylla-Spears, D. Edgell, M. J. Edwards, D. Fittinghoff, M. A. Barrios Garcia, A. Hamza, R. Hatarik, H. Herrmann, M. Hohenberger, D. Hoover, J. L. Kline, G. Kyrala, B. Koziolowski, G. Grim, J. E. Field, J. Frenje, N. Izumi, M. Gatun Johnson, S. F. Khan, J. Knauer, T. Kohut, O. Landen, F. Merrill, P. Michel, A. Moore, S. R. Nagel, A. Nikroo, T. Parham, R. R. Rygg, D. Sayre, M. Schneider, D. Shaughnessy, D. Strozzi, R. P. J. Town, D. Turnbull, P. Volegov, A. Wan, K. Widmann, C. Wilde, and C. Yeaman, “Inertially confined fusion plasmas dominated by alpha-particle self-heating,” *Nat. Phys.* **12**, 800–806 (2016).
- ²O. A. Hurricane, P. T. Springer, P. K. Patel, D. A. Callahan, K. Baker, D. T. Casey, L. Divol, T. Döppner, D. E. Hinkel, M. Hohenberger, L. F. Berzak Hopkins, C. Jarrott, A. Kritcher, S. Le Pape, S. Maclaren, L. Masse, A. Pak, J. Ralph, C. Thomas, P. Volegov, and A. Zylstra, “Approaching a burning plasma on the NIF,” *Phys. Plasmas* **26**, 052704 (2019).
- ³O. A. Hurricane, D. A. Callahan, D. T. Casey, P. M. Celliers, C. Cerjan, E. L. Dewald, T. R. Dittrich, T. Döppner, D. E. Hinkel, L. F. B. Hopkins, J. L. Kline, S. Le Pape, T. Ma, A. G. MacPhee, J. L. Milovich, A. Pak, H.-S. Park, P. K. Patel, B. A. Remington, J. D. Salmonson, P. T. Springer, and R. Tommasini, “Fuel gain exceeding unity in an inertially confined fusion implosion,” *Nature* **506**, 343–348 (2014).
- ⁴P. A. Jaanimagi and D. K. Bradley, “Neutron-streak- and framing-camera diagnostics for ICF implosions,” *Nucl. Instrum. Methods Phys. Res. A* **335**, 547–552 (1993).
- ⁵J. A. Frenje, T. J. Hilsabeck, C. W. Wink, P. Bell, R. Bionta, C. Cerjan, M. Gatun Johnson, J. D. Kilkenny, C. K. Li, F. H. Séguin, and R. D. Petrasso, “The magnetic recoil spectrometer (MRS) for time-resolved measurements of the neutron spectrum at the National Ignition Facility (NIF),” *Rev. Sci. Instrum.* **87**, 11D806 (2016).
- ⁶C. Bellei, P. A. Amendt, S. C. Wilks, M. G. Haines, D. T. Casey, C. K. Li, R. Petrasso, and D. R. Welch, “Species separation in inertial confinement fusion fuels,” *Phys. Plasmas* **20**, 012701 (2013).
- ⁷A. Inglebert, B. Canaud, and O. Larroche, “Species separation and modification of neutron diagnostics in inertial-confinement fusion,” *Eur. Phys. Lett.* **107**, 65003 (2014).
- ⁸V. A. Smalyuk, H. F. Robey, D. T. Casey, D. S. Clark, T. Döppner, S. W. Haan, B. A. Hammel, A. G. MacPhee, D. Martinez, J. L. Milovich, J. L. Peterson, L. Pickworth, J. E. Pino, K. Raman, R. Tipton, C. R. Weber, K. L. Baker, B. Bachmann,

- L. F. B. Hopkins, E. Bond, J. A. Caggiano, D. A. Callahan, P. M. Celliers, C. Cerjan, S. N. Dixit, M. J. Edwards, S. Felker, J. E. Field, D. N. Fittinghoff, N. Gharibyan, G. P. Grim, A. V. Hamza, R. Hatarik, M. Hohenberger, W. W. Hsing, O. A. Hurricane, K. S. Jancaitis, O. S. Jones, S. Khan, J. J. Kroll, K. N. Lafortune, O. L. Landen, T. Ma, B. J. MacGowan, L. Mase, A. S. Moore, S. R. Nagel, A. Nikroo, A. Pak, P. K. Patel, B. A. Remington, D. B. Sayre, B. K. Spears, M. Stadermann, R. Tommasini, C. C. Widmayer, C. B. Yeaman, J. Crippen, M. Farrell, E. Giraldez, N. Rice, C. H. Wilde, P. L. Volegov, and M. G. Johnson, "Mix and hydrodynamic instabilities on NIF," *J. Instrum.* **12**, C06001 (2017).
- ⁹T. Ma, P. K. Patel, N. Izumi, P. T. Springer, M. H. Key, L. J. Atherton, M. A. Barrios, L. R. Benedetti, R. Bionta, E. Bond, D. K. Bradley, J. Caggiano, D. A. Callahan, D. T. Casey, P. M. Celliers, C. J. Cerjan, J. A. Church, D. S. Clark, E. L. Dewald, T. R. Dittrich, S. N. Dixit, T. Döppner, R. Dylla-Spears, D. H. Edgell, R. Epstein, J. Field, D. N. Fittinghoff, J. A. Frenje, M. Gatu Johnson, S. Glenn, S. H. Glenzer, G. Grim, N. Guler, S. W. Haan, B. A. Hammel, R. Hatarik, H. W. Herrmann, D. Hicks, D. E. Hinkel, L. F. Berzak Hopkins, W. W. Hsing, O. A. Hurricane, O. S. Jones, R. Kauffman, S. F. Khan, J. D. Kilkenny, J. L. Kline, B. Koziolowski, A. Kritcher, G. A. Kyrala, O. L. Landen, J. D. Lindl, S. Le Pape, B. J. MacGowan, A. J. Mackinnon, A. G. MacPhee, N. B. Meezan, F. E. Merrill, J. D. Moody, E. I. Moses, S. R. Nagel, A. Nikroo, A. Pak, T. Parham, H.-S. Park, J. E. Ralph, S. P. Regan, B. A. Remington, H. F. Robey, M. D. Rosen, J. R. Rygg, J. S. Ross, J. D. Salmonson, J. Sater, D. Sayre, M. B. Schneider, D. Shaughnessy, H. Sio, B. K. Spears, V. Smalyuk, L. J. Suter, R. Tommasini, R. P. J. Town, P. L. Volegov, A. Wan, S. V. Weber, K. Widmann, C. H. Wilde, C. Yeaman, and M. J. Edwards, "The role of hot spot mix in the low-foot and high-foot implosions on the NIF," *Phys. Plasmas* **24**, 056311 (2017).
- ¹⁰V. A. Thomas and R. J. Kares, "Drive asymmetry and the origin of turbulence in an ICF implosion," *Phys. Rev. Lett.* **109**, 075004 (2012).
- ¹¹H. Azechi, N. Miyanaga, R. O. Stapf, H. Takabe, A. Nishiguchi, M. Unemoto, Y. Shimada, M. Yamanaka, T. Yamanaka, S. Nakai, and C. Yamanaka, "Thermonuclear burn time and duration in laser-driven high-aspect-ratio targets," *Appl. Phys. Lett.* **55**, 945–947 (1989).
- ¹²R. A. Lerche, D. W. Phillion, and G. L. Tietbohl, "25 ps neutron detector for measuring ICF target burn history," *Rev. Sci. Instrum.* **66**, 933 (1995).
- ¹³H. Sio *et al.*, *Rev. Sci. Instrum.* **87**, 11D701 (2016).
- ¹⁴Y. Arikawa *et al.*, *J. Phys.: Conf. Ser.* **112**, 032082–032085 (2008).
- ¹⁵C. Stoeckl, V. Yu. Glebov, S. Roberts, T. C. Sangster, R. A. Lerche, R. L. Griffith, and C. Sorce, "Ten-inch manipulator-based neutron temporal diagnostic for cryogenic experiments on OMEGA," *Rev. Sci. Instrum.* **74**, 1713 (2003).
- ¹⁶H. Geppert-Kleinrath, H. W. Herrmann, Y. H. Kim, A. B. Zylstra, K. Meaney, F. E. Lopez, B. J. Pederson, J. Carrera, H. Khater, C. J. Horsfield, M. S. Rubery, S. Gales, A. Leatherland, A. Meadowcroft, T. Hilsabeck, J. D. Kilkenny, R. M. Malone, J. D. Hares, A. K. L. Dymoke-Bradshaw, J. Milnes, and C. McFee, "Pulse dilation gas Cherenkov detector for ultra-fast gamma reaction history at the NIF," *Rev. Sci. Instrum.* **89**, 101146 (2018).
- ¹⁷T. Shimizu *et al.*, *Rev. Sci. Instrum.* **81**, 033102 (2010).
- ¹⁸H. Brysk, "Fusion neutron energies and spectra," *Plasma Phys.* **15**(7), 611 (1973).
- ¹⁹N. H. Matlis, G. R. Plateau, J. van Tilborg, and W. P. Leemans, "Single-shot spatiotemporal measurements of ultrashort THz waveforms using temporal electric-field cross correlation," *J. Opt. Soc. Am. B* **28**(1), 23–27 (2011).
- ²⁰J. Shan, A. S. Weling, E. Knoesel, L. Bartels, M. Bonn, A. Nahata, G. A. Reider, and T. F. Heinz, "Single-shot measurement of terahertz electromagnetic pulses by use of electro-optic sampling," *Opt. Lett.* **25**, 426 (2000).
- ²¹M. Nakajima, A. Namai, S. Ohkoshi, T. Suemoto, "Ultrafast time domain demonstration of bulk magnetization precession at zero magnetic field ferromagnetic resonance induced by terahertz magnetic field," *Opt. Express* **18**, 18260–18268 (2010).
- ²²K. Yamaguchi, M. Nakajima, and T. Suemoto, "Coherent control of spin precession motion with impulsive magnetic fields of half-cycle terahertz radiation," *Phys. Rev. Lett.* **105**, 237201 (2010).
- ²³Y. Minami, T. Kurihara, K. Yamaguchi, M. Nakajima, and T. Suemoto, "Longitudinal THz wave generation from an air plasma filament induced by a femtosecond laser," *Appl. Phys. Lett.* **102**, 151106 (2013).
- ²⁴T. Kurihara, H. Watanabe, M. Nakajima, S. Karube, K. Oto, Y. Otani, and T. Suemoto, "Macroscopic magnetization control by symmetry breaking of photoinduced spin reorientation with intense terahertz magnetic near field," *Phys. Rev. Lett.* **120**, 107202 (2018).
- ²⁵U. Schmidhammer, V. De Waele, J.-R. Marquès, N. Bourgeois, and M. Mostafavi, "Single shot linear detection of 0.01–10 THz electromagnetic fields: Electro-optic sampling with a supercontinuum in balanced detection," *Appl. Phys. B* **94**, 95–101 (2009).
- ²⁶Y. Okayasu, H. Tomizawa, S. Matsubara, N. Kumagai, A. Maekawa, M. Uesaka, and T. Ishikawa, "Feasibility study of a single-shot 3D electron bunch shape monitor with an electro-optic sampling technique," *Phys. Rev. Spec. Top. - Accel. Beams* **16**, 052801 (2013).
- ²⁷R. Pompili, M. P. Anania, F. Bisesto, M. Botton, M. Castellano, E. Chiadroni, A. Cianchi, A. Curcio, M. Ferrario, M. Galletti, Z. Henis, M. Petrarca, E. Schleifer, and A. Zigler, "Femtosecond dynamics of energetic electrons in high intensity laser-matter interactions," *Sci. Rep.* **6**, 35000-1–35000-7 (2016).
- ²⁸B. Ruiz, M. Jazbinsek, and P. Günter, "Crystal growth of DAST," *Cryst. Growth Des.* **8**(11), 4173–4184 (2008).
- ²⁹K. Niita, T. Sato, H. Iwase, H. Nose, H. Nakashima, and L. Sihver, "PHITS-A particle and heavy ion transport code system," *Radiat. Meas.* **41**, 1080–1090 (2006).
- ³⁰J. A. Frenje, R. Bionta, E. J. Bond, J. A. Caggiano, D. T. Casey, C. Cerjan, J. Edwards, M. Eckart, D. N. Fittinghoff, S. Friedrich, V. Y. Glebov, S. Glenzer, G. Grim, S. Haan, R. Hatarik, S. Hatchett, M. G. Johnson, O. S. Jones, J. D. Kilkenny, J. P. Knauer, O. Landen, R. Leeper, S. L. Pape, R. Lerche, C. K. Li, A. Mackinnon, J. McNaney, F. E. Merrill, M. Moran, D. H. Munro, T. J. Murphy, R. D. Petraso, R. Rygg, T. C. Sangster, F. H. Séguin, S. Sepke, B. Spears, P. Springer, C. Stoeckl, and D. C. Wilson, "Diagnosing implosion performance at the National Ignition Facility (NIF) by means of neutron spectrometry," *Nucl. Fusion* **53**, 043014 (2013).
- ³¹H. W. Herrmann, N. Hoffman, D. C. Wilson, W. Stoeffl, L. Dauffy, Y. H. Kim, A. McEvoy, C. S. Young, J. M. Mack, C. J. Horsfield, M. Rubery, E. K. Miller, and Z. A. Ali, "Diagnosing inertial confinement fusion gamma ray physics," *Rev. Sci. Instrum.* **81**, 10D333-1–10D333-5 (2010).
- ³²H. G. Rinderknecht, M. G. Johnson, A. B. Zylstra, N. Sinenian, M. J. Rosenberg, J. A. Frenje, C. J. Waugh, C. K. Li, F. H. Séguin, R. D. Petraso, J. R. Rygg, J. R. Kimbrough, A. MacPhee, G. W. Collins, D. Hicks, A. Mackinnon, P. Bell, R. Bionta, T. Clancy, R. Zacharias, T. Döppner, H. S. Park, S. LePape, O. Landen, N. Meezan, E. I. Moses, V. U. Glebov, C. Stoeckl, T. C. Sangster, R. Olson, J. Kline, and J. Kilkenny, "A novel particle time of flight diagnostic for measurements of shock- and compression-bang times in D³He and DT implosions at the NIF," *Rev. Sci. Instrum.* **83**, 10D902-1–10D902-5 (2012).
- ³³M. J.-E. Manuel, N. Sinenian, F. H. Séguin, C. K. Li, J. A. Frenje, H. G. Rinderknecht, D. T. Casey, A. B. Zylstra, R. D. Petraso, and F. N. Beg, "Mapping return currents in laser-generated Z-pinch plasmas using proton deflectometry," *Appl. Phys. Lett.* **100**, 203505 (2012).
- ³⁴F. Girard, L. Suter, O. Landen, D. Munro, S. Regan, and J. Kline, "NIF unconverted light and its influence on DANTE measurements," *Rev. Sci. Instrum.* **80**, 063104 (2009).
- ³⁵H. Takabe, M. Yamanaka, K. Mima, C. Yamanaka, H. Azechi, N. Miyanaga, M. Nakatsuka, T. Jitsuno, T. Norimatsu, M. Takagi, H. Nishimura, M. Nakai, T. Yabe, T. Sasaki, K. Yoshida, K. Nishihara, Y. Kato, Y. Izawa, T. Yamanaka, and S. Nakai, "Scalings of implosion experiments for high neutron yield," *Phys. Fluids* **31**, 2884 (1988).
- ³⁶N. Sinenian, A. B. Zylstra, M. J.-E. Manuel, H. G. Rinderknecht, J. A. Frenje, F. H. Séguin, C. K. Li, R. D. Petraso, V. Goncharov, J. Delettrez, I. V. Igumenchev, D. H. Froula, C. Stoeckl, T. C. Sangster, D. D. Meyerhofer, J. A. Cobble, and D. G. Hicks, "Total energy loss to fast ablator-ions and target capacitance of direct-drive implosions on OMEGA," *Appl. Phys. Lett.* **101**, 114102 (2012).